Symmetry Controlled, Genetic Presentation of Bioactive Proteins on the P22 Virus-like Particle Using an External Decoration Protein

Benjamin Schwarz,[†] Patrick Madden,[‡] John Avera,[†] Bridget Gordon,[§] Kyle Larson,[∥] Heini M. Miettinen,[∥] Masaki Uchida,[†] Ben LaFrance,[‡] Gautam Basu,[⊥] Agnieszka Rynda-Apple,[∥] and Trevor Douglas*[,†]

[†]Department of Chemistry, Indiana University, 800 E. Kirkwood Avenue, Bloomington, Indiana 47405, United States, [‡]Department of Chemistry and Biochemistry, Montana State University, PO Box 173400, Bozeman, Montana 59717, United States, [§]BiOptix Inc., 1775 38th Street, Boulder, Colorado 80301, United States, [∥]Department of Microbiology and Immunology, Montana State University, PO Box 173520, Bozeman, Montana 59717, United States, and [⊥]Department of Biophysics, Bose Institute, Kolkata 700054, India

ABSTRACT Viruses use spatial control of constituent proteins as a means of manipulating and evading host immune systems. Similarly, precise spatial control of proteins encapsulated or presented on designed nanoparticles has the potential to biomimetically amplify or shield biological interactions. Previously, we have shown the ability to encapsulate a wide range of guest proteins within the virus-like particle (VLP) from *Salmonella typhimurium* bacteriophage P22, including antigenic proteins from human pathogens such as influenza. Expanding on this robust encapsulation strategy, we have used the trimeric decoration protein (Dec) from bacteriophage L as a means of controlled exterior presentation on the mature P22 VLP, to which it binds with high affinity. Through genetic fusion to the C-terminus of the Dec protein, either the 17 kDa soluble region of murine CD40L or a minimal peptide designed from the binding region of the "self-marker" CD47 was independently presented on the P22 VLP capsid exterior. Both candidates retained function when presented as a Dec-fusion. Binding of the Dec domain to the P22 capsid was minimally changed across designed constructs, as measured by surface plasmon resonance, demonstrating the broad utility of this presentation strategy. Dec-mediated presentation offers a robust, modular means of decorating the exposed exterior of the P22 capsid in order to further orchestrate responses to internally functionalized VLPs within biological systems.

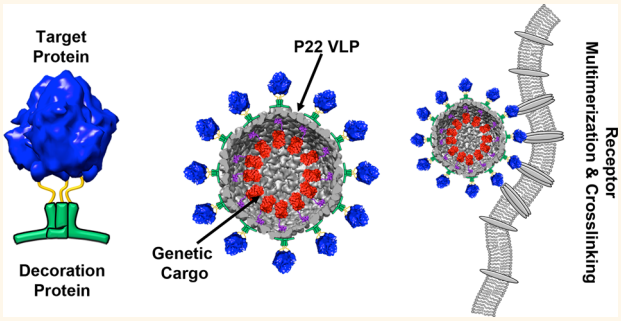

KEYWORDS: virus-like particle · CD40L (CD154) · polyvalent display · SPR · bacteriophage P22 · bacteriophage L decoration protein (dec)

The nanoarchitectures of viruses and other pathogens have evolved to infect, evade, and manipulate host cells while, in response, immune recognition of antigens and other molecular patterns has evolved to be highly dependent on valency.[1,2] Nanoengineering efforts have sought to mimic this same spatial scaffolding for biomedical applications of synthetic materials. One such effort has directly utilized virus-like particles (VLPs), which are inherently multivalent and possess multiple interfaces for functionalization.[3,4]

VLPs are noninfectious nanocage architectures derived from viral sources or other naturally occurring protein cage architectures. These cages can be isolated from infectious viruses by removing nucleic acid cargo or, in some cases, expressed heterologously. VLPs have been shown to act as effective scaffolds for nanoengineering applications including imaging, catalysis, materials construction, cellular targeting and vaccinology.[1,3,5−9] All aspects of a VLP structure are genetically coded and engineering efforts can take advantage of their inherent self-assembly and genetic programmability by utilizing existing VLP proteins to direct protein cargo to different interfaces of the capsid. Here we demonstrate a robust strategy for presentation on the exterior of the VLP from *Salmonella typhimurium* bacteriophage P22

* Address correspondence to trevdoug@indiana.edu.

Received for review June 3, 2015 and accepted August 12, 2015.

Published online August 12, 2015
10.1021/acsnano.5b03360

complementing previous genetic encapsulation strategies and providing a modular, genetic, interior and exterior functionalized VLP system.

The P22 VLP adopts an approximately 60 nm $T = 7$ icosahedral structure assembled from 420 copies of the 46 kDa coat protein and as many as 300 copies of the 34 kDa scaffolding protein.[10] The VLPs spontaneously assemble *in vivo* after heterologous coexpression of these two proteins.[11] Guest proteins can be directed for encapsulation by genetic fusion to the scaffold protein.[12,13] Initially the VLP adopts a spherical procapsid (PC) morphology but upon heating to 65 °C undergoes a structural transformation to an expanded form (EX), which closely resembles the expansion of the infectious virus during DNA packaging.[14]

Guest encapsulation within the P22 VLP, either scaffold protein-directed or *via* synthetic bioconjugation, has shown potential for biomedical applications such as diagnostic magnetic resonance imaging and vaccine development.[9] In particular, previous work, using a mouse model, has shown that intranasal administration of P22 with encapsulated influenza nucleoprotein provides CD8+ T-cell mediated homosubtypic and heterosubtypic immunity, against lethal infections with PR8 and X31 influenza viruses.[15]

Development of a similar genetic strategy for exterior presentation would allow for the construction of spatially controlled bifunctional particles. The P22 VLP tolerates extension of the C-terminus of the coat protein resulting in externally functionalized particles.[16] However, presentation of large protein species is problematic as the C-termini are likely sterically crowded at local 5- and 6-fold vertices. Viral decoration proteins, which bind at symmetry specific sites on the exterior of the capsid, offer a biomimetic alternative to direct fusion to the coat protein.

Decoration proteins are common in double-stranded DNA bacteriophages and examples include Soc protein from bacteriophage T4, gpD in bacteriophage lambda, and Dec in bacteriophage L.[17−21] These accessory coat proteins can serve as structural reinforcement for the capsid architecture.[18] Of these decoration proteins, gpD has been used to present proteins, including multimers, on the surface of the lambda capsid with applications in phage display selection.[22,23]

While bacteriophage P22 lacks a native decoration protein, the trimeric decoration protein (Dec), from the highly similar bacteriophage L, binds with high affinity to the mature P22 capsid.[21,24] The naturally occurring pro-heads for both bacteriophage L and P22 show no evidence for Dec binding,[21] which suggests that binding is discriminatory toward the EX morphology. Structural studies show that Dec binds preferentially to EX at the quasi-3 fold site but also occupies the true 3-fold site with lower affinity, suggesting that slight asymmetry in the topology of the binding site has a large impact on binding.[24,25]

From cryo-EM reconstruction models, the C-terminus of Dec was found to project away from the capsid surface at the center of the trimer providing a potentially useful conjugation site.[25] We constructed multiple Dec fusion proteins and truncations to test the utility of this system for ligand presentation. The Dec protein was fused to either the minimal CD47 peptide (Self) or the 17 kDa soluble region of murine CD40L. Self is a 21-amino acid peptide developed by Discher and co-workers from the contacting residues between CD47 and its binding partner SIRP-α.[26] The Self-peptide is able to bind to SIRP-α and inhibit phagocytosis by macrophages in the same manner as CD47.[27,28] Presentation of Self-peptide on the capsid surface may extend capsid circulation time within the body.

CD40L (CD154), a transmembrane signaling cytokine with a conserved TNF-like trimeric structure, is a key signal in adaptive immunity with applications as an adjuvant in infectious pathogens and cancer immunotherapy.[29−33] Polyvalent presentation of CD40L trimers, or other TNF family ligands, *via* the Dec trimer could lead to robust signaling and activation by promotion of native quaternary structure and high levels of polyvalent presentation.

We show that Dec presentation is largely unaffected by C-terminal fusion. Furthermore, Dec presentation can be used in conjunction with previously reported interior encapsulation *via* genetic fusion to the scaffold protein to create an inside- and outside-functionalized P22 VLP using only genetic means.[13] P22 loaded with mCherry-SP was imbued with affinity for B lymphocytes through decoration with DecCD40L. In addition, uptake of P22 labeled with Cy7 by splenocytes was decreased through decoration with DecSelf thus demonstrating the versatility of the platform.

We have also analyzed the mechanism and kinetics of binding providing key insights into further engineering of the Dec system. By Surface Plasmon Resonance (SPR) we distinguished between the contributions of a tighter and weaker interaction demonstrating subnanomolar affinity in the highest affinity interaction, nearly 3 orders of magnitude tighter than previous estimates. We demonstrated that the P22-Dec interactions, localized to the Dec N-terminal region, are likely charge-mediated and that the binding interaction can be modulated by ionic strength. Additionally, we identify a novel Dec-binding particle population within heterologously expressed P22-VLPs that may represent semiconserved defect particles.

RESULTS AND DISCUSSION

The C-Terminus of Dec Tolerates Large Protein Fusions. In order to facilitate the designed presentation of proteins on the surface of the P22 capsid, cargo proteins were linked to the C-terminus of the Dec protein *via* genetic fusion (Figure 1). As a structurally simple case, the small, monomeric Self-peptide was introduced to

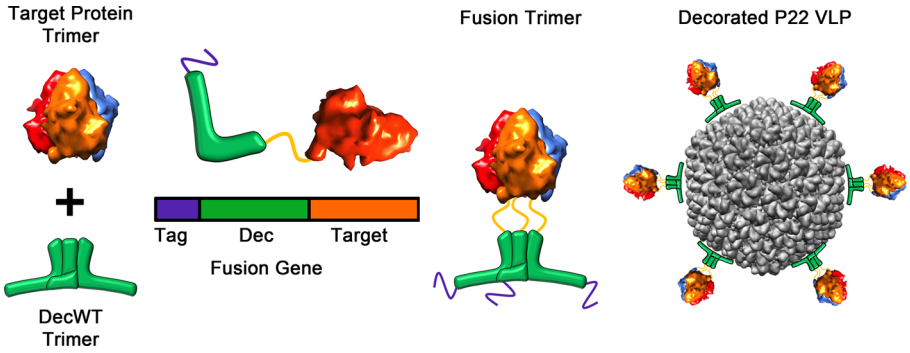

Figure 1. Dec-facilitated ligand presentation uses genetic fusion of a target-protein to the C-terminus of Dec (green). A poly histidine tag (purple) is maintained on the N-terminus of Dec for purification. Heterologous expression and purification results in a soluble trimeric Dec fusion. The Dec construct can then be used to decorate an EX-P22 sample (gray) by mixing the two components. Images were generated using PDB entries 1ALY and 2XYZ.

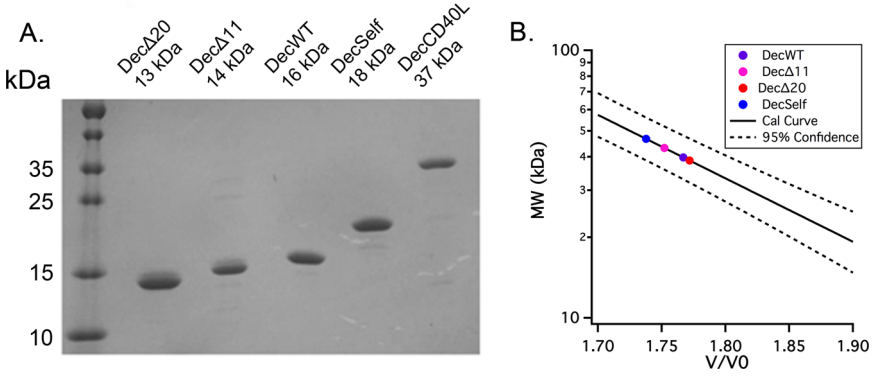

Figure 2. Dec constructs are readily expressed and purified as soluble trimers. (A) SDS-PAGE analysis shows a single band for each Dec construct at the expected molecular weight after Ni-affinity chromatography. (B) Calibrated analytical size-exclusion chromatography reveals that DecWT, DecΔ11, DecΔ20 and DecSelf all exist as trimers in solution. DecCD40L interacted with the column and was not analyzed.

form the DecSelf construct.[26] To examine the potential for Dec to present large multimeric proteins, the 148 amino acid soluble region of murine CD40L (AA 112−260), was cloned from a mouse thymus cDNA source and fused to the C-terminus of the Dec protein forming a DecCD40L fusion construct. The C3 symmetric structure of CD40L matches that of the underlying Dec, potentially enabling a strain free arrangement during assembly, binding and presentation. All genetic constructs were confirmed by DNA sequencing.

Both of these constructs, as well as DecWT, were expressed heterologously in *E. coli* and purified *via* an N-terminal 6× histidine tag. Both chimeric Dec constructs were expressed as soluble proteins although a significant portion of DecCD40L was observed by SDS-PAGE in the insoluble cell debris following lysis. Lowering the expression temperature to room temperature following induction resulted in higher yields of soluble DecCD40L. The purity of each construct was assessed by SDS-PAGE. After two passes through nickel-NTA chromatography all samples showed a single band at the expected molecular weight for DecWT (16 175 Da), DecSelf (18 320 Da) and DecCD40L (36 871 Da) (Figure 2A). All constructs were stable for at least 3 months at 4 °C.

Previous reports have shown, by sedimentation equilibrium analysis, that DecWT exists as a trimer in solution.[21] We used calibrated analytical size exclusion chromatography (SEC) to examine the quaternary structure of the Dec constructs. DecWT displayed a single peak at 40 ± 3 kDa, which corresponds well to a trimeric state (43.7 kDa). DecSelf displayed a single peak at 47 ± 3 kDa, which also matches a trimeric state (51.5 kDa) (Figure 2B). DecSelf was reanalyzed after storage at 4 °C for 4 weeks and exhibited higher molecular weight peaks. To examine the contribution of a cysteine residue in Self-peptide to these higher molecular weight species, the same analysis was performed in the presence of 33 mM DTT. The addition of reductant resulted in the complete disappearance of the higher molecular weight peaks, which shifted to the trimeric peak (data not shown). Analysis of the DecCD40L was complicated due to an apparent interaction with the column preventing accurate measurement of the quaternary state by SEC. Further functional studies and surface plasmon resonance (SPR) fitting, discussed later, suggest that the functional trimeric state of CD40L is maintained. Taken together these data suggest that Dec can maintain a trimeric structure in the presence of C-terminal fusion.

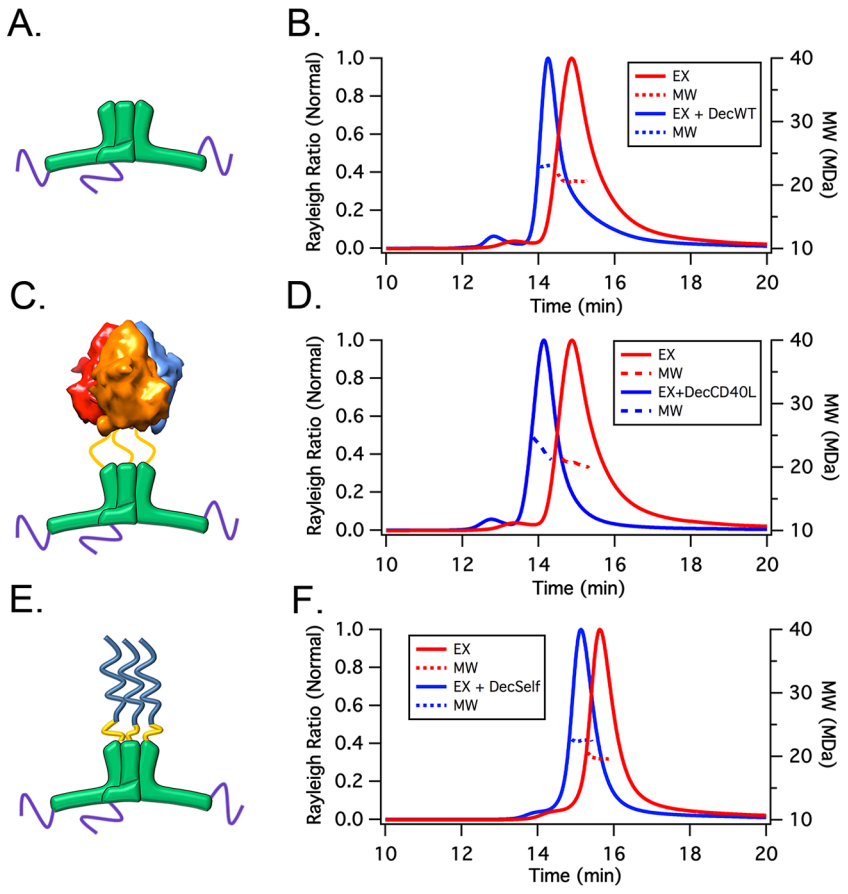

Figure 3. Dec tolerates C-terminal extension through genetic fusion. (A) A representation of the Dec trimer showing the central pillar capped with a cluster of the C-termini. (B) DecWT binding to EX P22 results in a particle molecular weight shift of 2.5 MDa and a retention time shift of 0.62 min as measured by SEC-MALS. (C) DecCD40L incorporates the C3 symmetric mCD40L at the C-terminus allowing for maintenance of the quaternary structure of both components. (D) DecCD40L binding results in a retention shift of 0.73 min and molecular weight increase of 1.9 MDa. Only 0.8 equiv of DecCD40L per available site could be bound and analyzed by MALS due to interactions between DecCD40L and the column. (E) DecSelf incorporates a short monomeric peptide at the C-terminus. (F) DecSelf shows a similar molecular weight increase (2.1 MDa) and retention shift (0.5 min) on binding. The DecCD40L representation utilizes PDB 1ALY.

Future applications of this system may require alternative methods such as S-carboxymethylation to block potential interprotein disulfide formation and avoid particle aggregation.

DecCD40L and DecSelf Show Binding to the P22 VLP. An initial assessment of in-solution binding of Dec constructs to the EX P22 VLP was made using size-exclusion chromatography (SEC) coupled with multi-angle and quasi-elastic light scattering (MALS and QELS) respectively. Binding of DecWT to the capsid resulted in a shift in retention time and increase in hydrodynamic radius (r_h) of ~1 nm suggesting an increase in the size of the particle. By MALS, the particle mass increased by 2.5 ± 0.2 MDa corresponding to 155 ± 6 DecWT monomers (Figure 3A,B, Table 1). This number suggests partial occupancy with a total expected occupancy of 180 monomers at the 60 quasi-3-fold sites and 60 monomers at the 20 true-3-fold sites for a total possible site occupancy of 240 Dec monomers. It should be noted that SEC-MALS is not appropriate to monitor the actual stoichiometry of binding as there is an ~15 min delay between when the sample is taken out of equilibrium with excess Dec and when it is detected

TABLE 1. Global Particle Molecular Weight (MW), Radius of Hydration (Rh) And Retention Shift of P22 upon Dec Binding Were Measured by SEC Coupled to MALS and QELS[a]

construct	MW (MDa)	Dec monomers	Rh (nm)	retention shift (min)
EX	20.5 ± 0.2	0 ± 12	28.4 ± 0.7	0 ± 0.008
EX+DecWT	23.0 ± 0.1	155 ± 6	29.6 ± 0.7	0.619 ± 0.005
EX+DecΔ11	23.6 ± 0.2	214 ± 14	30.1 ± 0.7	0.595 ± 0.005
EX+DecΔ20	20.5 ± 0.2	0 ± 15	28.6 ± 0.6	0.076 ± 0.009
EX+DecCD40L[b]	22.4 ± 0.2	51 ± 5	30.2 ± 0.7	0.729 ± 0.008
EX+DecSelf	22.6 ± 0.2	114 ± 11	29.6 ± 0.8	0.500 ± 0.005
PC	22.8 ± 0.7	0 ± 43	26.4 ± 0.5	0 ± 0.001
PC+DecWT	23.2 ± 0.2	24 ± 14	26.6 ± 0.7	0.03 ± 0.008

[a] The number of Dec monomers was calculated *via* the difference between bound and control particle molecular weight. All uncertainty reflects one standard deviation. For EX and PC controls "Dec monomer" standard deviation reflects the number of DecWT monomers. [b] The DecCD40L sample was incubated with less than a full equivalent of the DecCD40L construct per anticipated Dec site due to interactions of DecCD40L with the column. This also introduces significant uncertainty into the retention shift for this construct.

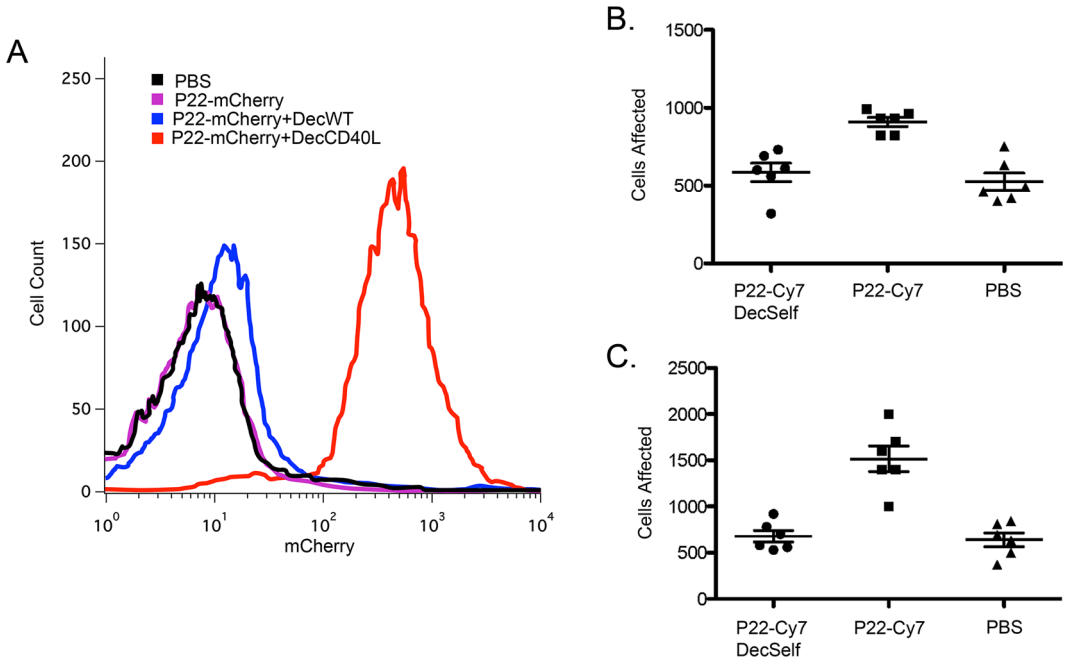

Figure 4. DecCD40L and DecSelf retain activity against primary cells. (A) P22-mCherry decorated with DecCD40L (red) showed binding to primary B-lymphocytes while P22-mCherry (purple) and P22-mCherry decorated with DecWT (blue) show minimal difference from a PBS control. (B) P22-Cy7 decorated with DecSelf showed minimal association with splenocytes compared to naked P22-Cy7 when incubated at 37 °C ($P = 0.0006$ P22-Cy7 *vs* P22-Cy7 + DecSelf; $P = 0.0001$ P22-Cy7 *vs* PBS). (C) Incubation of the same samples at 4 °C results in similar patterns associated with adhesion to splenocytes ($P = 0.0002$ P22-Cy7 *vs* P22-Cy7 + DecSelf; $P = 0.0002$ P22-Cy7 *vs* PBS). All error bars reflect one standard deviation.

as it elutes off the column. For these reasons this technique is only used as an initial assessment of interaction between the Dec constructs and the capsid.

To assess the effect of either CD40L or Self-peptide fusion on Dec binding, in-solution binding was assessed in the same manner as DecWT (Figure 3C,E). By SEC and QELS both constructs showed retention shifts and increases in the r_h of 1.8 and 1.2 nm for DecCD40L and DecSelf, respectively. By MALS, increases in particle molecular weight were observed corresponding to the binding of 51 ± 5 DecCD40L and 114 ± 11 DecSelf monomers (Figure 3D,F, Table 1). The lower occupancy for these constructs may indicate decreased binding or steric hindrance of adjacent sites. In the case of DecCD40L decreased occupancy is more likely due to the lower number of equivalents of DecCD40L that were used with this sample to avoid the interactions with the column that prevented analytical SEC analysis. SPR results discussed later suggest that both DecCD40L and DecSelf occupy approximately the same number of sites as DecWT.

CD40L Maintains CD40 Binding in P22-Bound State. In addition to maintaining binding to the capsid, target proteins must maintain functionality. To assess the functionality of the CD40L domain, DecCD40L was assayed for binding to primary murine B lymphocytes that display CD40 in high abundance.[29,33,34] To avoid phagocytosis of the particles, independent of CD40L-CD40 binding, all incubations were done at 4 °C. DecCD40L was bound in excess to EX capsids containing an mCherry-SP fusion protein encapsulated on the interior.[13] CD40L decorated mCherry-P22 incubated with naive murine primary B lymphocytes ($B220^+$, $CD19^+$) showed dramatic increases in binding, assessed by fluorescence-activated cell sorting, compared to P22 alone or P22 functionalized with DecWT, suggesting that the CD40L domain is functional as a fusion to Dec and presented on the surface of P22 (Figure 4A).

Similar to other TNF family signaling mechanisms, CD40 requires trimerization by CD40L before it can associate with the trimeric, cytosolic TNF receptor-associated factors (TRAF) 2 and 3.[31,35−38] Previous attempts to utilize the soluble region of CD40L to stimulate the immune system have shown promise but are limited by the dose required to elicit an effect. This is likely due to the absence of avidity interactions and receptor clustering present in native CD40-CD40L signaling.[31,39] Efforts to utilize antibodies as high-affinity alternatives to CD40L and TNF family ligands have also fallen short of promoting robust signaling because the bivalent binding of antibodies does not promote trimerization of CD40 without further cross-linking.[40]

Polyvalent presentation of CD40L on the capsid surface likely maintains quaternary structure while making multiple contacts with cell surface CD40 and may result in effective signaling. Further studies are needed to characterize the nature of immune stimulation by DecCD40L decorated VLPs. By delivering a mCherry-SP cargo this result also shows that Dec

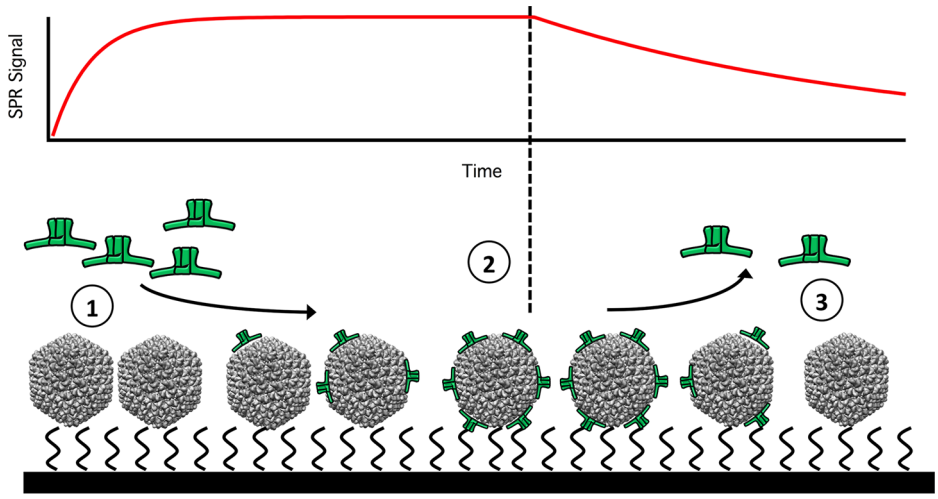

Figure 5. Dec-P22 binding measured by SPR utilizes an NHS/EDC immobilized EX P22 chip. Dec is applied to the chip at a known concentration (1) and binding is monitored by increasing SPR signal. After binding has been allowed to proceed the sample injection is switched to buffer (2). Dec release from P22 is observed by a decaying SPR signal (3). Both the association and dissociation phase are fit simultaneously to a binding model.

presentation can be utilized effectively with previously demonstrated scaffold protein-directed encapsulation resulting in a spatially controlled bifunctional VLP.

Self Successfully Inhibits Phagocytosis of P22. As discussed above, the Self-peptide is a minimal mimic of CD47, which is a known marker of self and inhibitor of phagocytosis by macrophages. To assess the ability of surface presented DecSelf to decrease particle uptake, decorated VLPs were incubated with primary splenocytes. For ease of detection, P22 particles were labeled internally with Cy7-maleimide. P22-Cy7 alone or P22-Cy7 decorated with DecSelf was incubated with splenocytes at 37 °C to encourage phagocytosis. Compared to P22-Cy7, DecSelf associated with cells with lower frequency ($P = 0.0006$) (Figure 4B). DecSelf association was indistinguishable from PBS controls suggesting minimal interaction. Binding experiments were also performed at 4 °C to assess particle association with the cell surface without uptake. Low temperature trends reflected the same patterns seen at 37 °C (Figure 4C). These results suggest that Self-peptide presented as a Dec fusion on the exterior of the P22 VLP remains functional, interrupting association and uptake of particles.

High Salt Can Reverse Dec Binding. While the above results showing maintenance of function during Dec presentation are encouraging, these cell incubations occur on a relatively short time scale. In order for the Dec presentation strategy to be useful *in vivo*, binding must be stable for hours to days. In addition, detailed understanding of both the strength and mechanism of binding is essential in order to further engineer the Dec system. Previously, fluorescence anisotropy and a single site equilibrium-binding model were used to estimate a K_D of 40−180 nM for Dec with an N-terminal his-tag.[25] We anticipated that by monitoring the kinetics of binding we could distinguish between the contributions of the two binding sites, assess the stability of the interaction and better understand overall the impact of engineering the Dec protein.

To monitor binding kinetics a SPR assay was developed. EX-P22 was immobilized *via* NHS/EDC coupling to the chip surface allowing for Dec to be flowed over the surface at known concentrations (Figure 5). Identification of regeneration conditions that interrupted the Dec-P22 interaction but left the immobilized P22 capsids intact was key to the development of a robust SPR assay. In addition to providing a required method for refreshing the chip surface, regeneration conditions also provided insight into the mechanism of Dec binding to the capsid. Multiple regeneration conditions were screened and pulsed addition of 4 M $MgCl_2$ was shown to completely regenerate the P22 bound surface without interrupting the immobilized capsid integrity (Figure S1A). The integrity of the capsid under these conditions was confirmed by SEC. P22 was stable in 4 M $MgCl_2$ though Dec was released from the capsid (Figure S1B). In contrast, other common regeneration conditions, 0.35 mM EDTA or 20% acetonitrile, did not affect the Dec-P22 interaction. Lower concentrations of $MgCl_2$ were screened as well as a range of LiCl concentrations. High concentrations of LiCl (7 M) resulted in complete regeneration but also caused loss of material from the SPR chip. Short pulses of lower concentrations of either $MgCl_2$ or LiCl resulted in only partial regeneration of the chip surface (data not shown). Disruption of the Dec-P22 interaction with high salt over the short 10 s pulses utilized here may suggest that the interaction is at least partially electrostatic. However, both $MgCl_2$ and LiCl are known to act as chaotropes and thus regeneration could also be the result of partial denaturation of the Dec protein or coat protein.

Dec Binds to the Capsid with Subnanomolar Affinity. To assess the kinetics of binding, DecWT was bound to the

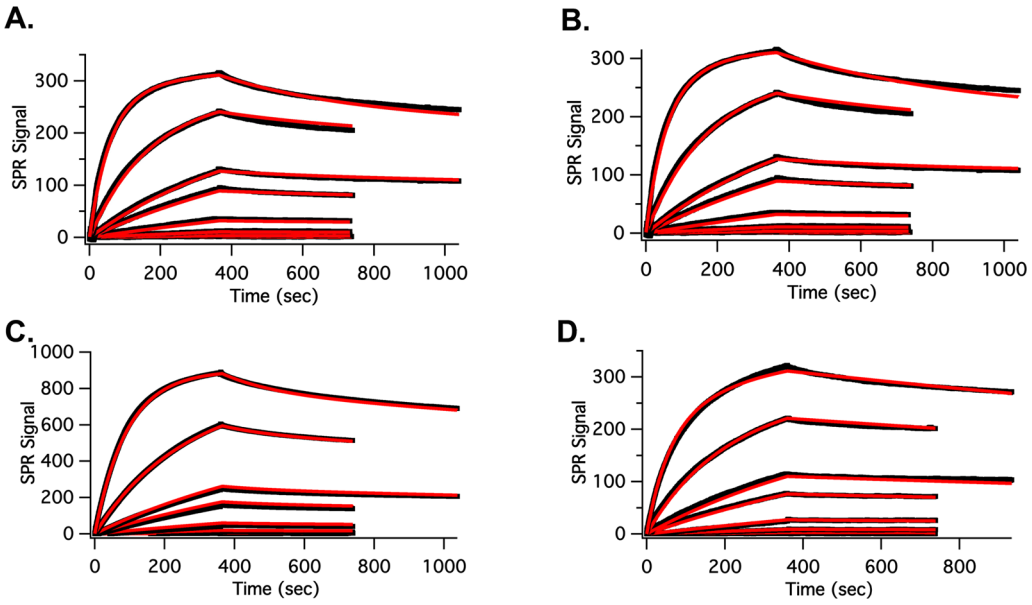

Figure 6. DecWT binding, measured by SPR, reflects biphasic behavior and low nanomolar affinity. DecCD40L and DecSelf are minimally affected by C-terminal fusion. (A) DecWT binding kinetics demonstrate biphasic behavior and are well fit to a two-site model. Application of the fit results in a high-affinity site K_D of 9.2 nM and a low-affinity site K_D of 1502 nM. (B) Two-site fit applied to the same concentration data set but with the tight site k_d held at 3.2×10^{-6} s^{-1} reflecting the results of the 4 h dissociation experiments. (C) DecCD40L binding kinetics, measured by SPR, demonstrate biphasic behavior and are well fit by a two-site model. Fits resulted in a high-affinity site K_D of 30.8 nM and a low-affinity site K_D 1,421 nM. (D) DecSelf kinetics also were well fit by a two-site model resulting in a high-affinity site K_D of 18.3 nM and a low-affinity site K_D 146 nM. For all SPR sets a single representative concentration set is displayed with data shown in black traces and fits overlaid in red. Each trace shows a binding sensorgram for a different concentration of Dec construct (1−1580 nM).

EX P22 surface at a range of concentrations and both the binding and dissociation were recorded by SPR. Initial binding measurements showed biphasic behavior consistent with two-site binding in the dissociation process at Dec concentrations as low as 100 nM. This involvement of the lower-affinity site potentially contributed to the high degree of uncertainty in the previous measurements.[25] For this reason, the true affinity of Dec for the high affinity site was anticipated to be higher than reported if the contributions of each site could be deconvoluted.

Accurate data-fitting required that each data set be fit globally across all concentrations and in triplicate. Common mistakes in global biphasic Langmuir fitting models lie in the numerous models that can describe biphasic behavior. Experimental factors that may cause apparent biphasic signals include heterogeneity of the surface or analyte sample as well as overloading of the ligand surface. These were avoided by extensive purification of Dec samples and the use of an isotropic virus particle as the immobilized ligand. Chip loading with P22 was carefully monitored in real-time and terminated at levels estimated to be below the threshold for mass-transport limitations eq 1. This was confirmed by the absence of characteristic linearity in the early association phase. A simple two-independent binding site model was anticipated based on previous reports showing Dec binding to both the 3-fold (low-affinity) and quasi-3-fold (high-affinity) sites of the P22 capsid.

Another factor complicating global fitting in general is the strong dependence on the initial input values. To avoid nondescriptive solutions, the data were fit systematically. First, low concentration data not displaying biphasic shape, at 100 nM Dec and below, were fit to a single-site binding model providing an initial estimate of association rate constants (k_a) and dissociation rate constants (k_d) (Figure S2, Table S1). Estimates for k_a and k_d were then used as inputs for the first site of a two-site binding model, initially held fixed and then allowed to vary after reasonable inputs had been obtained for the rate constants for the second site (k_{a2} and k_{d2}).

As anticipated, binding of DecWT over the full range of concentrations assayed was poorly fit by a single-site Langmuir model eq 3 but matched well with an expected two independent site Langmuir model (eq 4, Figure 6A). While the two sites of the capsid may not be truly independent, previous cryo-EM reconstructions showed no evidence to justify using a more complex allosterically connected two-site model. As expected DecWT was shown to bind with higher than reported affinity to the high-affinity binding site (k_a: 11 540 ± 30 M^{-1} sec^{-1}, k_d: 1.06 ± 0.06 × 10^{-4} s^{-1}, K_D: 9.2 ± 0.5 nM) and with micromolar affinity to a second lower affinity binding site (k_a: 1980 ± 146 M^{-1} sec^{-1}, k_d: 2.98 ± 0.06 × 10^{-3} s^{-1}, K_D: 1502 ± 115 nM). Low-concentration single-site fitting results were in agreement with the tighter binding site parameters from the two-site binding fit (k_a: 13 832 ± 93 M^{-1} sec^{-1}, k_d: 3.30 ± 0.03 × 10^{-4} s^{-1}, K_D: 24.0 ± 0.3 nM).

TABLE 2. SPR Kinetic Binding Parameters of Dec Constructs and Truncations for a Two-Site Binding Model[a]

construct	k_{a1} (M^{-1} s^{-1})	k_{d1} ($s^{-1} \times 10^{-4}$)	K_{D1} (nM)	k_{a2} (M^{-1} s^{-1})	k_{d2} ($s^{-1} \times 10^{-4}$)	K_{D2} (nM)
DecWT	11 540 ± 30	1.06 ± 0.06	9.2 ± 0.5	1980 ± 146	29.8 ± 0.6	1502 ± 115
DecWT[b]	12 561 ± 20	0.032	0.255 ± 0.004	4086 ± 32	18.2 ± 0.2	445.9 ± 5
DecΔ11	9203 ± 18	0.44 ± 0.06	4.8 ± 0.6	38 311 ± 349	44 ± 2	155 ± 8.7
DecΔ20	70.6 ± 0.3	2.4 ± 0.1	3450 ± 30	–	–	–
DecCD40L	6439 ± 4	2.0 ± 0.03	30.8 ± 0.4	4824 ± 93	68 ± 1	1421 ± 38
DecSelf	11 246 ± 80	2.0 ± 0.03	18.3 ± 0.3	2193 ± 109	32.3 ± 0.3	145.9 ± 7.3

[a] All parameters are the result of global fitting across three full concentration set replicates (1—1580 nM Dec). Error reflects one standard deviation as reported by the global fit utility in IGOR PRO. DecΔ20 parameters are the result of a single-site fit and concentrations sets spanning 31.6—31 600 nM. [b] The second set of DecWT parameters is the result of fitting with k_{d1} fixed at 3.2×10^{-6} s^{-1} reflecting 4 h dissociation runs.

Despite sensitivity to variation in all other parameters, the fit was insensitive to fixing the k_d of the tight site to lower values. This is not surprising as minimal curvature due to the tight site can be observed in the 10 min dissociation time of these runs (Figure 6A). Thus, parameter outputs of this initial fit serve only as maximum estimates for the k_d of this site and may not reflect the actual k_d. To better examine this parameter the dissociation of 10 μM injections of DecWT was monitored for 4 h and fit to a two-site model (Figure S3A). Significant reduction in the k_d for both sites were observed (k_{d1}: $3.20 \pm 0.04 \times 10^{-6}$ s^{-1}, k_{d2}: $9.50 \pm 0.05 \times 10^{-4}$ s^{-1}) (Figure 6B). Despite the extended run time there was still minimal curvature observed for the tight site suggesting that the k_d may be even lower. In addition, deviation from good fit was observed early in the run where the curvature due to lower affinity interactions is most evident. To examine this contribution a third set of site parameters was introduced into the fit, which accounted for the deviation (Figure S3B). This disagreement suggests an interaction that is more complex than an independent two-site model possibly due to sterics or allostery. Such an effect could be due to changes in the dynamics of the capsid upon binding such as seen with GpD and bacteriophage lambda.[41]

To assess the highest affinity interaction the k_d of the tight site was fixed in the two-site fit across the full concentration data set. Minimal deviation was seen in other parameters resulting in a K_D for the tight site of 0.255 ± 0.003 nM (Table 2). These parameters indicate a half-life of Dec binding at the tight site of at least 60 h. This affinity suggests that Dec constructs have the potential to stay associated with the P22-VLP for extended periods of time highlighting the potential utility of this system for *in vivo* applications.

Dec Binding is Largely Unaffected by C-Terminal Modification. Binding kinetics were measured for DecCD40L and DecSelf using the same immobilized P22 chip surface as for the DecWT experiments. Both constructs showed increased equilibrium signal at the same concentrations compared to DecWT indicating a larger mass deposition on the chip surface. Assuming that the same number of surface sites (P22) were available and being occupied, these results suggest that, as expected, the analyte had a larger molecular weight than DecWT. The binding of Dec constructs was compared to DecWT two-site fit without fixing the tight site k_d. Kinetic fitting of the DecCD40L showed minimal change in affinity at the tighter binding site (k_a: 6439 ± 4 M^{-1} sec^{-1}, k_d: $2.0 \pm 0.03 \times 10^{-4}$ s^{-1}, K_D: 30.8 ± 0.4 nM) and maintenance of the weaker binding site affinity despite the presence of the fused CD40L domain (Figure 6C, Table 2). As with DecWT, fitting of the low concentration data set for DecCD40L by a single site model resulted in agreement with the tighter-site parameters of the two-site model (Figure S2C).

DecSelf also maintained biphasic-binding behavior but the fit to a simple two-site model was not as robust as for DecWT or DecCD40L (Figure 6D). Nevertheless results for DecSelf binding to the tighter binding site (k_a: 11,246 ± 80 M^{-1} sec^{-1}, k_d: $2.0 \pm 0.03 \times 10^{-4}$ s^{-1}, K_D: 18.3 ± 0.3 nM) showed minimal change from DecWT (Table 2). Fit disagreement may be the result of some aggregation of DecSelf due to the cysteine in the Self-peptide as seen in the aged sample described above. DecSelf samples were prepared fresh for the SPR experiment and the uniformity assessed by SEC but any cross-linked species in the population formed subsequently could have contributed to fitting error.

As mentioned above, SEC MALS is not an ideal method for monitoring the relative occupancy of Dec constructs at the available sites of the capsid due to the delay time between the sample being taken out of equilibrium and being monitored. SPR has previously been used to compare the stoichiometry of interactions and an estimate of the relative occupancy was calculated from net R_{max} obtained from the kinetic fit of the SPR data. The net R_{max}, the sum of the R_{max} from the tight site and the weak site of the fit, reflects the projected maximum signal due to binding of the Dec construct to the EX-P22 surface. For the same chip surface R_{max} can be compared to give a relative occupancy based on the molecular weight of the construct. For DecCD40L the relative binding compared to DecWT was 2.61 ± 0.06 compared to the expected value of 2.28 based on the ratio of the construct MW. For DecSelf relative binding was calculated to be 0.94 ± 0.04 compared to the

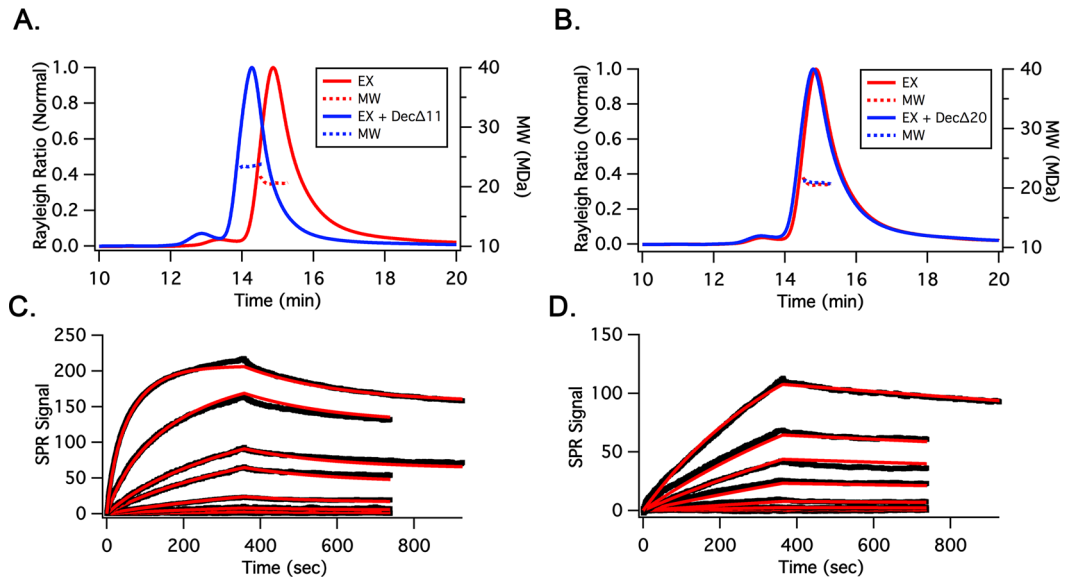

Figure 7. DecΔ20, but not DecΔ11, shows a severe reduction in binding to EX P22. (A) DecΔ11 binding to EX P22 results in a 3.1 MDa increase in particle mass and a 0.6 min shift in retention time as measured by SEC-MALS. (B) DecΔ20 incubation with EX P22 resulted in no mass increase or retention shift. (C) DecΔ11 binding kinetics, measured by SPR (1−1580 nM), were in good agreement with a two-site model resulting in a high-affinity site K_D of 4.8 nM and a low-affinity site K_D of 155 nM. (D) DecΔ20 binding kinetics (31.6-31,600 nM) only showed monophasic behavior over the concentrations examined resulting in a single-site K_D of 3.5 μM. Each trace in (C) and (D) shows a sensorgram of a different Dec construct concentration. For all SPR sets a single representative concentration set is displayed with data shown in black traces and fits overlaid in red.

expected value of 1.13 (Table S2). Discrepancies between the expected and calculated values could be the result of slight differences in occupancy but are more likely a consequence of slight disagreements in the fitting of the data to a simple two-site model. Taken together these results suggest that Dec tolerates large fusions at its C-terminus and, while there may be subtle differences in the binding behavior, largely maintains binding to the capsid.

Identification of Key Dec Binding Regions. To further examine the mode of Dec binding and in an effort to potentially identify intermediate affinity Dec mutants, truncations of either the first 11 (DecΔ11) or 20 (DecΔ20) N-terminal residues were generated and analyzed for stability and binding. By calibrated SEC, both the DecΔ11 and DecΔ20 showed only single peaks at 43 ± 3 and 39 ± 3 kDa respectively which best corresponded to a trimeric structure (43.4 and 40.3 kDa) (Figure 2B). This suggests that key trimerization residues for the Dec protein are not located in the N-terminal 20 residues. In-solution binding assessed by SEC-MALS-QELS showed that DecΔ11 binding results in increased particle molecular weight and a retention shift but binding of DecΔ20 is completely absent (Figure 7A,B, Table 1).

The kinetics of binding for both DecΔ11 and DecΔ20 were assessed by SPR. DecΔ11 bound with similar affinity to DecWT at both the tight and weak binding sites (Figure 7C, Table 2). DecΔ20 bound with significantly reduced affinity. DecΔ20 binding data did not display biphasic behavior over a concentration range of 0.032−31.6 μM. Fitting to a single-site model showed a more than 300-fold reduction in K_D from the high-affinity site of DecWT (Figure 7D, Table 2). The estimated relative occupancy for both constructs was assessed using the net R_{max}. Both DecΔ11 and DecΔ20 displayed less than expected binding relative to DecWT but, as mentioned above, this may be explained by deviations in the fit as opposed to actual reduced site occupancy. The constructs showed an expected progressive decrease in the net R_{max} with reduced MW (Table S2).

Amino acid sequences of the N-terminus were compared between DecWT, DecΔ11 and DecΔ20. Notably DecΔ20, but not DecΔ11, loses charged residues compared to DecWT (K14, D15 and D17). While there may also be contributions from loss of essential structure due to truncation, the loss of binding with the loss of charged sites is consistent with the observed reversibility of the Dec-P22 interactions at high ionic strength. Identification of key binding regions could allow for the development of Dec variants with intermediate affinity for the capsid. Dec has previously been shown to be useful in mediating the assembly of P22 into higher order structures.[42] Modulating the affinity of Dec linkers in these systems could provide a key control in the assembly process.

Disulfide Cross-Linked Dec Induced Aggregation Removes a PC-like Subpopulation. In initial examination of the Dec-P22 interaction it was found that a subpopulation of P22-PC binds Dec, in apparent contradiction of reports in the literature where Dec does not bind to the PC morphology (Figure 8A). This suggested that our sample (purified by ultracentrifugation and SEC)

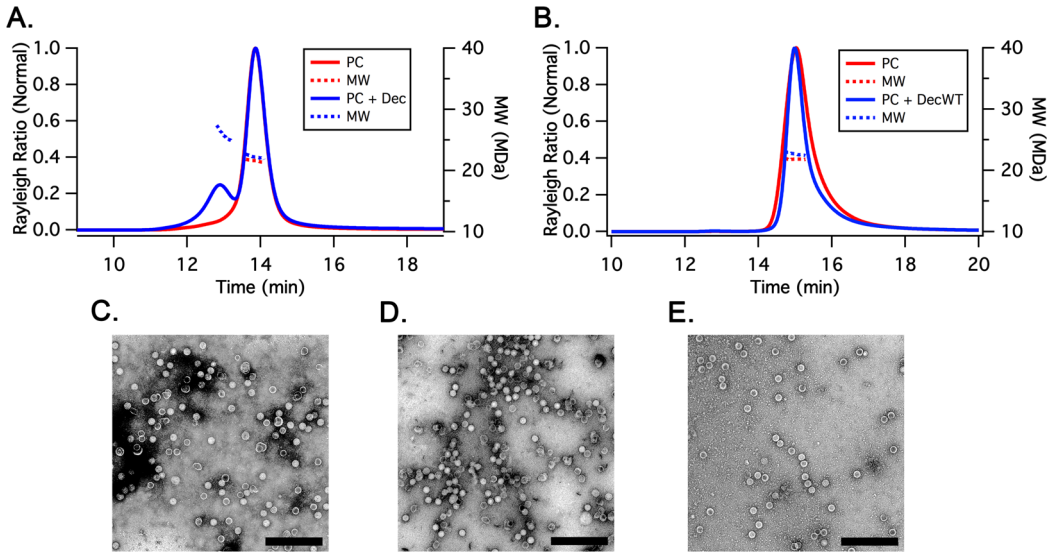

Figure 8. A P22 PC subpopulation was shown to bind Dec and could be removed through selective aggregation. (A) An initial purification of P22 PC exhibits the emergence of a higher molecular weight peak by SEC-MALS in the presence of excess Dec. (B) Following selective cross-linking of the binding population using a disulfide forming Dec mutant (DecS134C) the higher molecular weight peak is removed. (C) A TEM micrograph of PC sample prior to cross-linking shows well-formed particles in the presence of misformed particles. (D) A TEM micrograph of Dec cross-linking induced aggregate shows a high percentage of misformed particles. (E) The recovered supernatant after cross-linking shows nearly complete removal of the misformed particle population. All scale bars are 500 nm.

was contaminated with a subpopulation that could not be removed *via* our normal purification procedure. This provided an immediate problem for further analysis of Dec binding and required purification.

To remove the subpopulation from the PC sample we used a C-terminal cysteine mutant of Dec (DecS134C), which upon oxidation forms a linear head-to-head dimer of trimers that can cross-link and aggregate particles to which it binds.[42] The percentage of this subpopulation in the P22-PC sample was found to vary from batch to batch and could be purified away through Dec-Dec aggregation. The remaining PC was shown to have no measurable affinity for Dec (Figure 8B). Aggregated particles were resolubilized with 30 mM DTT and compared to nonaggregated particles by transmission electron microscopy (TEM). Particles in the aggregate showed higher frequency of cracked or incomplete particles compared with the original sample while the remaining particles after aggregation were almost completely devoid of misformed particles (Figure 8C–E).

This P22-PC subpopulation is indistinguishable by SEC, density-gradient ultracentrifugation and nondenaturing agarose gel electrophoresis (data not shown). Only TEM reveals the presence of the subpopulation, which is evident as mis-formed or incomplete particles. Formation of this subpopulation is likely a consequence of an imbalance in the relative production of coat protein and scaffold protein during heterologous expression. Aberrant assemblies of P22 have been reported and can usually be separated by centrifugation or SEC.[43] The subpopulation could also be due to a small amount of carry-over from an aberrant P22 peak that precedes the intact particle peak in nearly every heterologously expressed P22 VLP batch. However, given the quantity of these particles a more likely explanation is that the particles are imperfect $T = 7$ capsids that coelute with PC on SEC (Figure 8A). Interestingly the Dec binds extremely well to the aberrant assemblies and the Dec-Dec dimer precipitation was utilized as an effective method of purification.

CONCLUSIONS

We have shown that the bacteriophage L Dec protein can be used as a modular display tool for the presentation of complex protein moieties on the surface of the P22 VLP. Presentation of target proteins through fusion to the C-terminus of the Dec protein was shown to be robust and versatile. DecSelf presented on the VLP surface decreased cellular uptake during incubation with splenocytes and may provide a strategy for prolonging circulation of P22 VLP constructs in the body. DecCD40L, presented in the same fashion, showed drastically increased affinity for B lymphocytes suggesting that the trimeric protein is both presented and properly folded. In the DecCD40L experiments particles were tracked using a genetically incorporated interior payload of mCherry-SP demonstrating the compatibility of the two methods.

The Dec protein was shown to bind to high affinity sites on the P22 particle with higher affinity than previously reported. Two-site binding to the capsid surface, as suggested previously from cryo-EM reconstruction, was further supported by kinetic characterization of the binding process. As the concentration of Dec increases, evidence for a second weaker binding

behavior, to the true-3-fold sites of the capsid, becomes evident.

The N-terminal domain of Dec was shown to be responsible for binding to the capsid. Specifically the section from amino acid 11−20 was critical for the binding interaction. Binding of Dec was reversed at high ionic strength suggesting that the interaction is at least partially charge-mediated. This insight can be used to design Dec constructs with alternative binding affinities to the capsid, allowing for control over processes such as Dec-mediated higher order assembly of capsids or release of the Dec-cargo from the capsid under controlled conditions.[42] Building on previous studies, demonstrating the broad utility of the P22 VLP as a modular encapsulation system through scaffold protein-fusion, Dec exterior functionalization allows for a similar utility on the exterior capsid surface. The unique use of accessory proteins (scaffold protein and Dec) as bioconjugation strategies while leaving the capsid protein unmodified allows for the preservation of the core capsid structure and the potential to add more complex cargos. This is the first known example of a three-protein, completely genetic VLP scaffolding system for simultaneous protein display and encapsulation.

MATERIALS AND METHODS

Materials. DNA modifying enzymes were purchased from New England Biolabs and Promega. DNA primers were purchased from Eurofins MWG Operon. *Escherichia coli* chemically competent BL21(λDE3) and electro competent ClearColi cells were purchased from Lucigen. QIAquick gel extraction kit and QIAprep Spin Miniprep kit were purchased from Qiagen. Cy7-maleimide was purchased from LumiProbe. All other chemical reagents were purchased from Fisher Scientific.

Molecular Biology. The DecWT gene with an N-terminal 6× histidine tag was provided by Dr. Peter Prevelige and ligated into a pET Duet vector *via* *Bam*HI and SacI sites. The 21 amino acid CD47 mimic Self-peptide was synthesized as a codon-optimized, annealed primer-set with exposed SacI and *Hin*dIII sticky ends (Self-fwd and Self-rev) The Self-fragment was ligated into to the pET Duet DecWT vector. Proper stop codons were introduced *via* quick-change PCR using Self-stop fwd and Self-stop rev. The soluble region of mCD40L was cloned from a murine thymus and lymph node cDNA library, provided by Dr. Ed Schmidt (Montana State University), into the DecWT vector using introduced SacI and *Hin*dIII restriction sites (DecCD40L fwd and DecCD40L rev). Truncations of the first 11 or first 20 N-terminal residues were carried out using the Q5 Site-Directed Mutagenesis Kit according to the manufacturer's instructions (New England Biolabs, catalog# E0554) using Dec Δ11 fwd, DecΔ20 fwd and pET rev. The DecWT pETDuet plasmid was used as template DNA. All inserts and mutations were confirmed by DNA sequencing (Eurofins MWG Operon, Inc.).

Self-fwd: 5′-cggcaactatacctgcgaagtgaccgaactgacccgcgaaggcgaaaccattattgaaCTGAAAA-3′.

Self-rev: 5′-agcttTTTCAGTTCAATAATGGTTTCGCCTTCGCGGGTCAGTTCGGTCACTTCGCAGGTATAGTTGCCgagct-3′.

Self-stop fwd: 5′-cgaaaccattattgaactgaaataaaagcttgcggccgca-3′.

Self-stop rev: 5′-tgcggccgcaagcttttatttcagttcaataatggtttcg-3′.

DecCD40L fwd: 5′- tatgagctccaaagaggtgatgaggatcctcaa-3′.

DecCD40L rev: 5′-Tataagctttcagagtttgagtaagccaaaagatg-3′.

Dec Δ11 fwd: 5′-CTATACAAAGATGCTGACGGTGTATATGTGTCTGC-3′.

pET rev: 5′-CGGATCCTGGCTGTGGTGATGATG-3′.

DecΔ20 fwd: 5′-GTGTCTGCGCTTCCGATTAAAGCTATCAAATACG-3′.

Expression, Lysis and Purification. All constructs were transformed into either BL21 (DE3) *E. coli* or Clear Coli. *E. coli* strains harboring expression vectors for the Dec constructs were grown on LB medium at 37 °C in the presence of ampicillin or kanamycin to maintain selection for the plasmid. Expression of the genes was induced by addition of isopropyl β-D-thiogalactopyranoside (IPTG) to a final concentration of 0.5 mM once the cells reached mid log phase (OD600 = 0.6). Cultures of DecSelf, DecCD40L and DecΔ11 were cooled to room temperature before induction in order to encourage a higher percentage of soluble product during purification. Cultures were grown for 4 h after addition of IPTG, then the cells were harvested by centrifugation and cell pellets stored at −20 °C overnight. Using ClearColi all constructs were expressed as above but overnight growth was extended from 8 to 16 h to account for the approximately 40 min doubling time of the ClearColi strain.

Cell pellets were resuspended in PBS (50 mM sodium phosphate, 100 mM sodium chloride, pH 7.0) with lysozyme, DNase and RNase added and incubated at room temperature for 30 min. For Dec constructs, 1 protease inhibitor minitablet (Roche) was added per liter of original culture. The cell suspension was lysed by sonication. Cellular components were removed by centrifugation at 12000*g* for 45 min at 4 °C. **P22:** P22 samples were purified from the postlysis supernatant by ultracentrifugation through a 5 mL 35% (w/v) sucrose cushion. The resulting viral pellet was resuspended in PBS (50 mM sodium phosphate, 100 mM sodium chloride, pH 7.0) and centrifuged at 16000*g* for 20 min to remove any remaining aggregates. Samples were then purified over an S-500 Sephadex (GE Healthcare Life Sciences) size exclusion column using a Biorad Biologic Duoflow FPLC. Fractions containing P22 were concentrated by ultracentrifugation and the resulting viral pellet was resuspended in an adequate volume of PBS or HBS (50 mM HEPES, 100 mM NaCl, pH 7.0). **Dec:** All His-tagged constructs were purified using a 5 mL Roche cOmplete His-tag purification column. Samples were loaded onto the column in PBS at 2 mL/min and washed with 40 mL of 50 mM phosphate, 100 mM sodium chloride, 20 mM imidazole pH 7.5. Samples were eluted with an 80 mL gradient from 20 to 125 mM imidazole. Fractions were collected based on A_{280} and the pooled fractions were dialyzed into PBS or HBS overnight. Samples were concentrated by rebinding to His-tag column, washing with 40 mL of 20 mM imidazole and stepwise elution with 250 mM imidazole in either PBS or HBS. Samples were dialyzed as before to remove imidazole. Concentrations of each construct were determined by UV absorption measured at 280 nm under denatured conditions (5 M guanidine hydrochloride) using extinction coefficients calculated using Protein Calculator v3.3 (Chris Putnam, Scripps).

P22 Expansion. Procapsid P22 was diluted in PBS to a final concentration of 1.5 mg/mL and heated in a water bath at 67 °C for 25 min. Expansion was assessed *via* nondenaturing 1% agarose gel electrophoresis at 65 V for 2 h in TAE buffer (40 mM Tris, 20 mM acetate, 1 mM EDTA pH 8.0) stained with Coomassie blue. Expanded samples were subsequently concentrated *via* ultracentrifugation

SDS-PAGE. Protein samples were mixed with 4× loading buffer containing 100 mM DTT, heated in a boiling water bath for 10 min, removed, and spun down on a benchtop centrifuge. Samples were separated on a 15% acrylamide gel at a constant current of 35 mA for approximately 1 h. Gels were stained with Coomassie blue stain, rinsed with water, and destained. Images were recorded on a UVP MultDoc-IT Digital Imaging System. A 10−180 kDa PageRuler prestained ladder was used for reference.

Analytical Size Exclusion Chromatography. Calibrated analytical SEC was performed on a WTC-030S5 (Wyatt Technologies) column on an Agilent 1200 HPLC at 0.7 mL/min of 50 mM phosphate, 100 mM sodium chloride and 200 ppm sodium azide pH 7.4. Samples at concentration of ∼1 mg/mL were

applied in 25 μL injections and detected by absorbance at 280 nm. The void volume was determined using both EX-P22 (MW: 19.6 MDa) and blue dextran (MW: 2 MDa). A calibration curve was established using a Sigma-Aldrich Gel Filtration Molecular Weight Markers Kit including equine cytochrome C (12.4 kDa), bovine carbonic anhydrase (29 kDa), bovine serum albumin (66 kDa), yeast alcohol dehydrogenase (150 kDa) and sweet potato β-amylase (220 kDa). Dec samples were run in triplicate and data were fit using IGOR Pro 6.3.

Multiangle Light Scattering. Samples were separated over a WTC-200S5 (Wyatt Technologies) size exclusion column and an Agilent 1200 HPLC at 0.7 mL/min of 50 mM phosphate, 100 mM sodium chloride and 200 ppm sodium azide pH 7.4. All capsid samples, with the exception of DecCD40L, bound with Dec constructs were incubated for 30 min in 3× stoichiometric excess of the respective Dec construct prior to injection. DecCD40L bound P22 was incubated with 0.8 equiv of DecCD40L per capsid site due to interactions of the DecCD40L with the column that prevented higher loading in this technique. Total run time was 30 min with injection of 25 μL per run. Resultant peaks were detected using a UV−vis detector (Agilent), a Wyatt HELEOS Multi Angle Laser Light Scattering (MALS) and detector, and an Optilab rEX differential refractometer (Wyatt Technology Corporation). The number-average particle molecular weight, Mn, was calculated across each peak half max with Astra 5.3.14 software (Wyatt Technology Corporation) using a previously calculated d*n*/d*c* value of 0.185 mL/g.

Surface Plasmon Resonance. A carboxymethyl dextran surface was functionalized with EX P22 through NHS/EDC coupling. Immobilization levels were estimated to allow for an approximate R_{max} of 250 RU during DecWT binding according to eq 1 where S is the number of binding sites per ligand.

$$R_{Ligand} = \left(\frac{MW_{Ligand}}{MW_{Analyte}}\right) \times R_{max} \times (1/S) \quad (1)$$

EX P22 ligand was dialyzed into 20 mM formate pH 4.4 and diluted to concentration of 10 μg/mL before being immobilized to a response level of 2000−2500 RU. For PC controls, PC P22 was immobilized to ∼4000 RU to account for increased mass and anticipated lack of binding. Previously reported binding parameters and preliminary assays were used to establish a relevant range of analyte dilutions from 0.316 to 1580 nM for DecWT. For extended dissociation runs, 10 μM DecWT was injected for 3 min and then buffer was run for 4 h before the chip was regenerated. All protein concentration measurements were taken under denatured conditions with an Agilent 8453 UV−vis spectrophotometer. Extinction coefficients were calculated using the Protein Calculator tool v3.4 developed by Chris Putnam at the Scripps Research Institute. All SPR measurements were performed using a Bioptix 404PI 4-channel instrument utilizing in-line reference cells to account for bulk effects and nonspecific binding.

Surface Plasmon Resonance Data Fitting. All data were fit using a user-defined protocol in IGOR Pro 6.3. Data were fit systematically to ensure reasonable initial guesses as input parameters. First the dissociation data at low analyte concentrations, exhibiting only monophasic behavior, were fit independently to a single-site model providing an initial input for the dissociation rate constant (k_d) of the high affinity site eq 2.

$$R(t; t_0 < t) = R_0 e^{-k_d(t - t_0)} \quad (2)$$

where R is SPR signal, R_0 is the initial signal intensity as dissociation begins, t_0 is the beginning of the dissociation phase. The single-site k_d estimate was initially held constant then allowed to vary in a fit of both the single site on and off rates for the low analyte concentration data set eq 3.

$$R(t) = \begin{cases} \frac{R_{max}[A]}{K_D + [A]}\left[1 - e^{-(k_a[A] + k_d)}\right] & 0 \le t \le t_0 \\ R_0 e^{-k_d(t - t_0)} & t_0 < t \end{cases} \quad (3)$$

where R_{max} is the signal at saturation or full site occupancy, k_a is the association rate constant, [A] is the concentration of analyte (Dec) and K_D (k_d/k_a) is the dissociation constant. The single-site estimates were then used as inputs for the high affinity site in an additive two-site model fit eq 4.

$$R(t) = \begin{cases} \frac{R_{max1}[A]}{K_{D1} + [A]}\left[1 - e^{-(k_{a1}[A] + k_{d1})}\right] + \frac{R_{max2}[A]}{K_{D2} + [A]}\left[1 - e^{-(k_{a2}[A] + k_{d2})}\right] & 0 \le t \le t_0 \\ R_{01} e^{-k_{d1}(t - t_0)} + R_{02} e^{-k_{d2}(t - t_0)} & t_0 < t \end{cases} \quad (4)$$

The association intensities at $t = t_0$ for each specific site, $R_1(t_0)$ or $R_2(t_0)$, are utilized as R_{01} and R_{02} in the dissociation fit at each iteration of the fit to eliminate discontinuity.

Extended dissociation runs were fit to the dissociation of two-independent sites consisting of a sum of two copies of eq 2. Fitting was offset from the switch from sample to buffer injection by 5 s to avoid contributions of residual bulk refractive index shifts.

For all fits, parameters were only restricted to non-negative values unless specifically indicated. All data sets were simultaneously fit globally and in triplicate to account for variance between instrument channels. All error is reported as one standard deviation as estimated by IGOR's global fit utility and reflects the uncertainty of the parameter within that specific fit and accompanying parameters.

Fluorescent Labeling. P22 S39C was treated with 5 mM DTT overnight and dialyzed twice into HBS. Sample was degassed by 4× pumping and refilling with argon. Cy7 maleimide was added to 2× excess and allowed to react overnight at 4 °C. Excess Cy7 was removed using 40k Zeba spin columns. Labeling was assessed by UV−vis according to manufacturer recommendations.

Primary Cell Assays Phagocytosis Assays. Primary cells were isolated from the spleen of a female BALB/c mouse. Red blood cells were lysed with ACK lysis buffer, and the primary cells were enumerated and diluted to a final concentration of 1×10^7 cells/mL. Cells were analyzed for the presence of B lymphocytes and 85% of cells were $B220^+$, $CD19^+$. Cells (1×10^6) were then transferred to a 48-well plate and allowed to synchronize on ice for 15 min after which capsid samples were added, 1 μg of P22 in each sample. For no-particle controls, 20 μL of PBS was added. The cells were again synchronized on ice for 15 min followed by a 60 min incubation at either 37 or 4 °C to analyze endocytosis and cell binding, respectively. For each set of assays (DecCD40L or DecSelf) a splenocyte extract of a single mouse was used for all replicates. Cells were analyzed with a FACSCanto (Becton, Dickinson and Company) and data were evaluated with FlowJo X (TreeStar).

Transmission Electron Microscopy. Samples (5 μL, 0.1 mg/mL protein) were applied to carbon-coated grids and incubated for 30 s. Excess liquid was wicked away with filter paper. Grids were then washed with 5 μL of distilled water. Grids were stained with 5 μL 2% Uranyl acetate and excess stain was wicked away with filter paper. Images were taken on a JEOL 1010 transmission electron microscope at accelerating voltage of 100 kV.

Conflict of Interest: The authors declare no competing financial interest.

Acknowledgment. We thank BiOptix Inc. for providing SPR instrumentation and technical support. We thank A. Wibowo and the Indiana University Physical Biochemistry Instrumentation Facility for their support in characterization and analysis. We thank P. Prevelige and S. Casjens for the Dec gene and E. Schmidt and J. Prigge for providing the mCD40L gene. This work was supported by NIH grants R01 AI104905 and R01 EB012027. B. Schwarz was supported by the Department of Defense (DoD) Air Force Office of Sponsored Research through the National Defense Science & Engineering Graduate Fellowship (NDSEG) Program

Supporting Information Available: The Supporting Information is available free of charge on the ACS Publications website at DOI: 10.1021/acsnano.5b03360.

Supplemental figures and tables, gene sequences, and fit code. (PDF)

REFERENCES AND NOTES

1. Grgacic, E. V. L; Anderson, D. A. Virus-Like Particles: Passport to Immune Recognition. *Methods* **2006**, *40*, 60–65.
2. Chackerian, B. Virus-Like Particles: Flexible Platforms for Vaccine Development. *Expert Rev. Vaccines* **2007**, *6*, 381–390.
3. Douglas, T.; Young, M. Viruses: Making Friends with Old Foes. *Science* **2006**, *312*, 873–875.
4. Uchida, M.; Klem, M. T.; Allen, M.; Suci, P.; Flenniken, M.; Gillitzer, E.; Varpness, Z.; Liepold, L. O.; Young, M.; Douglas, T. Biological Containers: Protein Cages as Multifunctional Nanoplatforms. *Adv. Mater.* **2007**, *19*, 1025–1042.
5. Garcea, R. L.; Gissmann, L. Virus-Like Particles as Vaccines and Vessels for the Delivery of Small Molecules. *Curr. Opin. Biotechnol.* **2004**, *15*, 513–517.
6. Comellas-Aragones, M.; Engelkamp, H.; Claessen, V. I.; Sommerdijk, N. A. J. M.; Rowan, A. E.; Christianen, P. C. M.; Maan, J. C.; Verduin, B. J. M.; Cornelissen, J. J. L. M.; Nolte, R. J. M. A Virus-Based Single-Enzyme Nanoreactor. *Nat. Nanotechnol.* **2007**, *2*, 635–639.
7. Pasqualini, R.; Ruoslahti, E. Organ Targeting *in vivo* Using Phage Display Peptide Libraries. *Nature* **1996**, *380*, 364–366.
8. Patterson, D. P.; Prevelige, P. E.; Douglas, T. Nanoreactors by Programmed Enzyme Encapsulation inside the Capsid of the Bacteriophage P22. *ACS Nano* **2012**, *6*, 5000–5009.
9. Lucon, J.; Qazi, S.; Uchida, M.; Bedwell, G. J.; LaFrance, B.; Prevelige, P. E., Jr; Douglas, T. Use of the Interior Cavity of the P22 Capsid for Site-Specific Initiation of Atom-Transfer Radical Polymerization with High-Density Cargo Loading. *Nat. Chem.* **2012**, *4*, 781–788.
10. Prevelige, P. E.; Fane, B. A. Building the Machines: Scaffolding Protein Functions During Bacteriophage Morphogenesis. In *Viral Molecular Machines*; Springer: Berlin, 2012; pp 325−350.
11. Prevelige, P. E.; Thomas, D.; King, J. Scaffolding Protein Regulates the Polymerization of P22 Coat Subunits into Icosahedral Shells *in vitro*. *J. Mol. Biol.* **1988**, *202*, 743–757.
12. Parker, M. H.; Casjens, S.; Prevelige, P. E. Functional Domains of Bacteriophage P22 Scaffolding Protein. *J. Mol. Biol.* **1998**, *281*, 69–79.
13. O'Neil, A.; Reichhardt, C.; Johnson, B.; Prevelige, P. E.; Douglas, T. Genetically Programmed *in vivo* Packaging of Protein Cargo and Its Controlled Release from Bacteriophage P22. *Angew. Chem., Int. Ed.* **2011**, *50*, 7425–7428.
14. Jiang, W.; Li, Z.; Zhang, Z.; Baker, M. L.; Prevelige, P. E.; Chiu, W. Coat Protein Fold and Maturation Transition of Bacteriophage P22 Seen at Subnanometer Resolutions. *Nat. Struct. Biol.* **2003**, *10*, 131–135.
15. Patterson, D. P.; Rynda-Apple, A.; Harmsen, A. L.; Harmsen, A. G.; Douglas, T. Biomimetic Antigenic Nanoparticles Elicit Controlled Protective Immune Response to Influenza. *ACS Nano* **2013**, *7*, 3036–3044.
16. Servid, A.; Jordan, P.; O'Neil, A.; Prevelige, P.; Douglas, T. Location of the Bacteriophage P22 Coat Protein C-Terminus Provides Opportunities for the Design of Capsid-Based Materials. *Biomacromolecules* **2013**, *14*, 2989–2995.
17. Qin, L.; Fokine, A.; O'Donnell, E.; Rao, V. B.; Rossmann, M. G. Structure of the Small Outer Capsid Protein, Soc: A Clamp for Stabilizing Capsids of T4-Like Phages. *J. Mol. Biol.* **2010**, *395*, 728–741.
18. Sae-Ueng, U.; Liu, T.; Catalano, C. E.; Huffman, J. B.; Homa, F. L.; Evilevitch, A. Major Capsid Reinforcement by a Minor Protein in Herpesviruses and Phage. *Nucleic Acids Res.* **2014**, *42*, 9096–9107.
19. Ishii, T.; Yamaguchi, Y.; Yanagida, M. Binding of the Structural Protein Soc to the Head Shell of Bacteriophage T4. *J. Mol. Biol.* **1978**, *120*, 533–544.
20. Lander, G. C.; Evilevitch, A.; Jeembaeva, M.; Potter, C. S.; Carragher, B.; Johnson, J. E. Bacteriophage Lambda Stabilization by Auxiliary Protein Gpd: Timing, Location, and Mechanism of Attachment Determined by Cryo-Em. *Structure* **2008**, *16*, 1399–1406.
21. Gilcrease, E. B.; Winn-Stapley, D. A.; Hewitt, F. C.; Joss, L.; Casjens, S. R. Nucleotide Sequence of the Head Assembly Gene Cluster of Bacteriophage L and Decoration Protein Characterization. *J. Bacteriol.* **2005**, *187*, 2050–2057.
22. Yang, F.; Forrer, P.; Dauter, Z.; Conway, J. F.; Cheng, N.; Cerritelli, M. E.; Steven, A. C.; Plückthun, A.; Wlodawer, A. Novel Fold and Capsid-Binding Properties of the Λ-Phage Display Platform Protein Gpd. *Nat. Struct. Biol.* **2000**, *7*, 230–237.
23. Gupta, A.; Onda, M.; Pastan, I.; Adhya, S.; Chaudhary, V. K. High-Density Functional Display of Proteins on Bacteriophage Lambda. *J. Mol. Biol.* **2003**, *334*, 241–254.
24. Tang, L.; Gilcrease, E. B.; Casjens, S. R.; Johnson, J. E. Highly Discriminatory Binding of Capsid-Cementing Proteins in Bacteriophage L. *Structure* **2006**, *14*, 837–845.
25. Parent, K. N.; Deedas, C. T.; Egelman, E. H.; Casjens, S. R.; Baker, T. S.; Teschke, C. M. Stepwise Molecular Display Utilizing Icosahedral and Helical Complexes of Phage Coat and Decoration Proteins in the Development of Robust Nanoscale Display Vehicles. *Biomaterials* **2012**, *33*, 5628–5637.
26. Rodriguez, P. L.; Harada, T.; Christian, D. A.; Pantano, D. A.; Tsai, R. K.; Discher, D. E. Minimal″ Self″ Peptides That Inhibit Phagocytic Clearance and Enhance Delivery of Nanoparticles. *Science* **2013**, *339*, 971–975.
27. Tsai, R. K.; Discher, D. E. Inhibition of "Self" Engulfment through Deactivation of Myosin-Ii at the Phagocytic Synapse between Human Cells. *J. Cell Biol.* **2008**, *180*, 989–1003.
28. Tsai, R. K.; Rodriguez, P. L.; Discher, D. E. Self Inhibition of Phagocytosis: The Affinity of 'Marker of Self'cd47 for Sirpα Dictates Potency of Inhibition but Only at Low Expression Levels. *Blood Cells, Mol., Dis.* **2010**, *45*, 67–74.
29. Schönbeck, U.; Libby, P. The Cd40/Cd154 Receptor/Ligand Dyad. *Cell. Mol. Life Sci.* **2001**, *58*, 4–43.
30. Banchereau, J.; Bazan, F.; Blanchard, D.; Brie, F.; Galizzi, J. P.; Van Kooten, C.; Liu, Y. J.; Rousset, F.; Saeland, S. The Cd40 Antigen and Its Ligand. *Annu. Rev. Immunol.* **1994**, *12*, 881–926.
31. Kwa, S.; Lai, L.; Gangadhara, S.; Siddiqui, M.; Pillai, V. B.; Labranche, C.; Yu, T.; Moss, B.; Montefiori, D. C.; Robinson, H. L. Cd40l-Adjuvanted DNA/Modified Vaccinia Virus Ankara Simian Immunodeficiency Virus Siv239 Vaccine Enhances Siv-Specific Humoral and Cellular Immunity and Improves Protection against a Heterologous Sive660 Mucosal Challenge. *J. Virol.* **2014**, *88*, 9579–9589.
32. Diehl, L.; den Boer, A. T.; Schoenberger, S. P.; van der Voort, E. I. H.; Schumacher, T. N. M.; Melief, C. J. M.; Offringa, R.; Toes, R. E. M. Cd40 Activation *in vivo* Overcomes Peptide-Induced Peripheral Cytotoxic T-Lymphocyte Tolerance and Augments Anti-Tumor Vaccine Efficacy. *Nat. Med.* **1999**, *5*, 774–779.
33. Van den Oord, J. J.; Maes, A.; Stas, M.; Nuyts, J.; Battocchio, S.; Kasran, A.; Garmyn, M.; De Wever, I.; De Wolf-Peeters, C. Cd40 Is a Prognostic Marker in Primary Cutaneous Malignant Melanoma. *Am. J. Pathol.* **1996**, *149*, 1953.
34. Law, C.-L.; Grewal, I. S. Therapeutic Interventions Targeting Cd40l (Cd154) and Cd40: The Opportunities and Challenges. In *Therapeutic Targets of the TNF Superfamily*; Springer: Berlin, 2009; pp 8−36.
35. Kuhné, M. R.; Robbins, M.; Hambor, J. E.; Mackey, M. F.; Kosaka, Y.; Nishimura, T.; Gigley, J. P.; Noelle, R. J.; Calderhead, D. M. Assembly and Regulation of the Cd40 Receptor Complex in Human B Cells. *J. Exp. Med.* **1997**, *186*, 337–342.
36. Fanslow, W. C.; Srinivasan, S.; Paxton, R.; Gibson, M. G.; Spriggs, M. K.; Armitage, R. J. Structural Characteristics of Cd40 Ligand That Determine Biological Function. *Semin. Immunol.* **1994**, *6*, 267–278.
37. McWhirter, S. M.; Pullen, S. S.; Holton, J. M.; Crute, J. J.; Kehry, M. R.; Alber, T. Crystallographic Analysis of Cd40 Recognition and Signaling by Human Traf2. *Proc. Natl. Acad. Sci. U. S. A.* **1999**, *96*, 8408–8413.
38. Pullen, S. S.; Labadia, M. E.; Ingraham, R. H.; McWhirter, S. M.; Everdeen, D. S.; Alber, T.; Crute, J. J.; Kehry, M. R. High-Affinity Interactions of Tumor Necrosis Factor Receptor-Associated Factors (Trafs) and Cd40 Require Traf Trimerization

and Cd40 Multimerization. *Biochemistry* **1999**, *38*, 10168–10177.
39. Stone, G. W.; Barzee, S.; Snarsky, V.; Santucci, C.; Tran, B.; Langer, R.; Zugates, G. T.; Anderson, D. G.; Kornbluth, R. S. Nanoparticle-Delivered Multimeric Soluble Cd40l DNA Combined with Toll-Like Receptor Agonists as a Treatment for Melanoma. *PLoS One* **2009**, *4*, e7334.
40. Gieffers, C.; Kluge, M.; Merz, C.; Sykora, J.; Thiemann, M.; Schaal, R.; Fischer, C.; Branschädel, M.; Abhari, B. A.; Hohenberger, P. Apg350 Induces Superior Clustering of Trail Receptors and Shows Therapeutic Antitumor Efficacy Independent of Cross-Linking *Via* Fcγ Receptors. *Mol. Cancer Ther.* **2013**, *12*, 2735–2747.
41. Hernando-Pérez, M.; Lambert, S.; Nakatani-Webster, E.; Catalano, C. E.; De Pablo, P. J. Cementing Proteins Provide Extra Mechanical Stabilization to Viral Cages. *Nat. Commun.* **2014**, 10.1038/ncomms5520.
42. Uchida, M.; LaFrance, B.; Broomell, C. C.; Prevelige, P. E.; Douglas, T. Higher Order Assembly of Virus-Like Particles (Vlps) Mediated by Multi-Valent Protein Linkers. *Small* **2014**, *11*, 1562.
43. Patterson, D. P.; Schwarz, B.; Waters, R. S.; Gedeon, T.; Douglas, T. Encapsulation of an Enzyme Cascade within the Bacteriophage P22 Virus-Like Particle. *ACS Chem. Biol.* **2013**, *9*, 359–365.